Proceedings of the Canadian Society for Mechanical Engineering International Congress 2021
CSME Congress 2021
June 27-30, 2021, Charlottetown, PE, Canada

Thermodynamic Modeling of Vortex Tubes Working with Real Gases

Ahmed Mansour
Mechanical Engineering Department
Université de Sherbrooke
Sherbrooke, Canada
ahmed.mansour@USherbrooke.ca

Junior Lagrandeur
Mechanical Engineering Department
Université de Sherbrooke
Sherbrooke, Canada
junior.lagrandeur@usherbrooke.ca

Sébastien Poncet
Mechanical Engineering Department
Université de Sherbrooke
Sherbrooke, Canada
Sebastien.Poncet@USherbrooke.ca

***Abstract*—A new real gas model is developed in order to estimate the cold and hot exit temperatures of a vortex tube. The effect of the Bödewadt boundary layer flow is considered in addition to the introduction of a correction factor to account for high cold mass fractions. The model predictions are compared to that of an ideal gas model and to experimental data available in the literature for three different refrigerants, namely air, R134a and carbon dioxide. The model exhibits similar results compared to the ideal gas model using air while it drastically improves the predictions of the cold and hot exit temperatures for R134a and carbon dioxide.**

***Index Terms*—vortex tube, real gas, carbon dioxide**

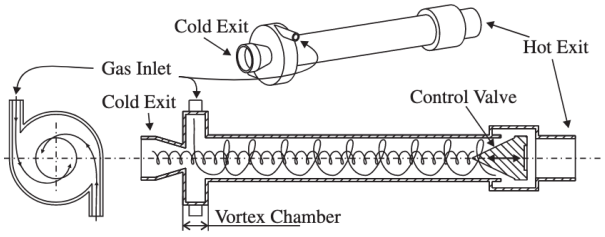

Fig. 1. A schematic representation of a counter-flow vortex tube [14]

I. Introduction

The main objective of the vortex tube is to separate a compressed gas into two streams, one at a lower temperature than the inlet temperature and the other at a higher temperature. This phenomenon is known as energy (temperature) separation. The vortex tube was first introduced by Ranque in the beginning of the 1930s [1]. But due to the poor available explanation of its working mechanism, it did not gain popularity in the scientific community at that time. In the mid-1940s, Hilsch [2] improved its design by trying to explain its working mechanism and the factors affecting its efficiency. A renew of interest is noted since the last few years due to its simplicity and its intriguing mechanism.

The vortex tube typically consists of multiple inlet nozzles and a main vortex chamber with two exits, the cold exit and the hot exit. There are two main configurations of vortex tube that are used due to their simplicity and they are distinguished by the locations of the orifices: the counter-flow (Fig. 1) and parallel-flow vortex tubes. A counter-flow vortex tube is mostly characterized by the placement of the cold exit and the inlets on one side of the tube while the hot exit is on the opposite end. For the parallel-flow design, the inlets are on one side while both the cold and hot exits are on the same other side. In general, the counter-flow vortex tube is more popular due to its better performance [3]. In a counter-flow vortex tube, passing through the tangential inlets, the fluid enters the vortex chamber producing a high swirling flow. This flow divides then into two streams, one leaving the tube through the hot exit along the periphery and the second flows along the axis towards the cold exit.

Ranque [1] came up with the explanation that the energy separation is caused by gas compression and expansion. Crocker et $al.$ [4] proposed that the core forced vortex is the main cause of pressure gradient across the tube diameter in the vortex tube with a high pressure region (compression) at the periphery and a low pressure zone (expansion) in the center. Hence, this may explain the temperature difference between the core and the periphery. Another theory emerged by the analysis of the flow structure. Hilsch [2] was the first to come up with the idea that internal friction is what causes the heat transfer from the inner core to the periphery. Fulton [5] proved that a free vortex exists at the periphery of the tube. Due to the presence of the forced vortex in the core, kinetic energy is transferred from the core to the periphery by friction between the different fluid layers. Due to this friction, a temperature difference emerges to make the core cooler and the periphery hotter. The secondary flow theory is based on the fact that part of the hot flow may expand into the cold flow stream at the plug end of the vortex tube and then moves back through the peripheral flow. Ahlborn and Groves [7] proved by experimental measurements that the mass flux through the cold exit is lower than that in the tube center. Hence, the secondary circulation is present apart from the primary vortex. In this process, the thermal energy is absorbed from the stream moving towards the cold exit and transferred back to the one moving towards the hot one [6]. One of the interesting theories explaining the temperature separation is the acoustic streaming. Kurosaka [8] proposed that the Rankine vortex transforms into a forced vortex due to acoustic streaming. By increasing the inlet pressure, the measured cold temperature

decreased. However, after reaching a certain pressure value, the temperature increased abruptly. As he was also measuring the sound pressure level, he also noticed an abrupt reduction in it. However, this theory is not fully valid for vortex tubes as he used a cylinder with the inlet and exit being on the same side [6].

Air is the most commonly used working fluid for fundamental studies about vortex tubes. However, most industrial applications require the use of other working fluids or refrigerants. As an example, the final objective of the present project is to optimize the performance of a transcritical CO_2 heat pump integrating a vortex tube. Thakare and Parekh [9] conducted a CFD study using air, nitrogen, carbon dioxide and oxygen. They came to the conclusion that nitrogen offers the maximum temperature difference between the hot and cold exits, while carbon dioxide leads to the minimum one. On the contrary, Agrawal et $al.$ [10] demonstrated experimentally that carbon dioxide performs the best compared to air and nitrogen in terms of cold temperature drop at a cold mass fraction of 0.3. Rafiee and Sadeghiazad [11] performed 3D CFD calculations using five different gases: air, nitrogen, oxygen, carbon dioxide and nitrogen dioxide. Based on their results, nitrogen dioxide showed the best capability to provide the maximum cooling and heating powers compared to the others while air exhibited the lowest performances. Kırmacı et $al.$ [12] made an exergy analysis using oxygen, nitrogen and argon. They conducted their experiments under a pressure range of $150 - 700$ kPa for different numbers of inlet nozzles and a fixed cold mass fraction of 0.5. Based on their results, argon showed the highest exergetic efficiency for every nozzle number and at all inlet pressures. On the other hand, nitrogen showed the maximum exergy losses among others gases even though air showed the lowest exergy efficiency.

Liew [13] developed an ideal gas model for vortex tubes with $L/D > 20$, where L and D are the vortex tube length and diameter, respectively. It also directly projects the effect of the pressure difference between the inlet and the exits to the estimations of exit temperatures. His model is based on the radial momentum equation, the perfect gas assumption and the isentropic flow relationships in the inlet nozzles. It relies on two main mechanisms. The first one explains the energy separation between the core and the periphery of the vortex tube based on the radial pressure gradient due to the centrifugal force. He explained that gas pockets expand and compress between the core and the periphery while transporting energy. The second mechanism is about the kinetic energy distribution throughout the vortex tube. He simply stated that the kinetic energy is higher in the periphery than in the core and that it converts into heat in the periphery. Liew [14] claimed that the average error between his model and his experiments is about 1.1% in terms of the exit temperatures. Lagrandeur et $al.$'s [21] model is based on that of Liew's with major improvements. Only the cold exit pressure is considered in this new model, friction losses are accounted for in the inlet nozzles and the Bödewadt boundary layer flow is added, having a significant effect especially for low cold mass fractions. They validated it with the experimental data of Camiré [20] and they showed that it greatly improves the former predictions of Liew [14].

The analytical models developed previously were dependent on the ideal gas assumption. However, these models are not suitable to work with real gases nor high pressure conditions. Hence a new model is required to provide more precise predictions working with such conditions. In this work, a new thermodynamic model is developed for real gases and to the best of the authors knowledge, it is the first one able to predict the two exit temperatures of a vortex tube.

II. Thermodynamic Model

A. Original Model

In order to develop the real gas model to be introduced in this section, the following parameters should be independent in order to calculate the exit temperatures:

- Total inlet pressure (P_{0in}) and temperature (T_{0in})
- Cold exit static pressure (P_c)
- Cold mass fraction (μ_c)
- Some geometrical dimensions: the radii of the vortex tube (r_{vt}), of the vortex chamber (r_{vc}) and of the cold exit (r_c)

In addition to that, some realistic assumptions and conditions are needed to simplify the model development:

- Compressible fluid
- Steady state flow
- The swirl velocity is much higher than the axial ($u_\theta >> u_z$) and radial ($u_\theta >> u_r$) components
- The change in the axial direction is neglected compared to that in the radial direction ($\frac{\partial}{\partial r} >> \frac{\partial}{\partial z}$)
- Isothermal static temperature along the inlet plane ($T_{in} \approx T_c$) [15]
- Fully developed turbulent flow in the cold exit
- Presence of a forced vortex
- Isentropic process in the inlet nozzles and cold exit

Accounting for the above mentioned assumptions, the radial momentum equation gets:

$$\frac{\partial P(r)}{\partial r} = \frac{u_\theta^2 \rho(r)}{r} \tag{1}$$

where P, r, u_θ and ρ are the static pressure (Pa), radius (m), swirl velocity (m/s) and density (kg/m^3), respectively. To solve this equation, a real gas equation of state (EoS) is needed. The ideal gas EoS is inaccurate at high operating pressures or low operating temperatures. In addition, not all fluids can be represented by the ideal gas law because their intermolecular forces become significant. Many equations were developed to account for the real gas behavior and they differ in their accuracy and sometimes complexity. In the present model, one considers the virial EoS, which can be expressed in either density or pressure series expansions:

$$\frac{PV_m}{RT} = 1 + \frac{B}{V_m} + \frac{C}{V_m^2} + \frac{D}{V_m^3} + ... \tag{2}$$

$$\frac{PV_m}{RT} = 1 + B^*P + C^*P^2 + D^*P^3 + ... \tag{3}$$

where V_m, T and R are the fluid's molar volume (m^3/mol), static temperature (K) and universal gas constant ($J/(mol.K)$). B (m^3/mol), C (m^6/mol^2), ..., called virial coefficients, are temperature-dependent. These coefficients are either determined experimentally or theoretically [16] and they represent the direct interactions between molecules [17]. Data available for the B coefficient are abundant and vary depending on the source for different gases and mixtures. Considering the C coefficient, the available data are less and exhibits higher uncertainties, while the available data for the other coefficients are almost scarce and the accuracy level is unknown from the measurements [17]. B^* and C^* are connected to the virial coefficients using the following equations:

$$B = B^* RT \tag{4}$$

$$C = (B^{*2} + C^*)(RT)^2 \tag{5}$$

The density series expansion is more fundamental, while pressure expansion is more practical. [18]. The pressure expansion series with the second and third virial coefficients is used in this work for the sake of its mathematical simplicity that complies with the developed model. As an integral part of the model, the swirl velocity is needed to be computed. Liew [13] could determine, experimentally and numerically, the behavior of the swirl velocity between the inlets and the cold exit. He, then, developed a mathematical representation of that velocity behavior in terms of the Mach number and the radius measured from the center line. The value of the Mach number increases linearly from the centerline till the vortex tube radius, then the value becomes constant till the vortex chamber radius. Instead of using the Mach number, the swirl velocity is used in the real gas model, and the mathematical representation becomes:

$$u_\theta(r) = \begin{cases} \omega_e r & 0 < r < r_{vt} \\ \omega_e r_{vt} & r_{vt} < r < r_{vc} \end{cases} \tag{6}$$

where ω_e is the rotational speed ($rev./s$) at the nozzle exits. Eqns. (3) and (6) are then combined with Eqn. (1). The pressure in the resultant equation is then integrated between the cold exit (P_c at $r = 0$) and the nozzles exit static pressure (P_{in} at $r = r_{vc}$) to get:

$$\begin{aligned} ln\left(\frac{P_{in}}{P_c}\right) + B^*\left(P_{in} - P_c\right) + \frac{C^*}{2}\left(P_{in}^2 - P_c^2\right) \\ = \frac{\omega_e^2 r_{vt}^2}{R_s T_{in}}\left(\frac{1}{2} + ln\left(\frac{r_{vc}}{r_{vt}}\right)\right) \end{aligned} \tag{7}$$

where T_{in} and R_s are the nozzles exit static temperature and the specific gas constant ($J/(kg.K)$), respectively.

When Liew [13] developed his equation that is parallel to Eqn. (7), he used the isentropic gas relations that were developed based on the ideal gas assumption to connect his equation to the inlet total pressure. Since such relations were not well-established using a real gas EoS, based on the authors' knowledge, and P_{in} is unknown, an iterative procedure is required to determine the rotational speed.

In order to obtain the exit temperatures of the vortex tube the following procedure is developed:

1) Using the inlet givens and with the help of the CoolProp database, the inlet total enthalpy and entropy are calculated.
2) The inlet static enthalpy (J/kg) can be computed at the nozzle exit using the total inlet enthalpy and the flow speed.

$$h_{in} = h_{0in} - \frac{\omega_e^2 r_{vt}^2}{2} \tag{8}$$

3) The values of T_{in} and P_{in} are then computed.
4) Using the value of T_{in} and iterating on the value of ω_e, P_{in} can be calculated using Eqn. (7).
5) The values of P_{in} from steps 3 and 4 are then compared with each other. The iterative process is repeated until both values are similar.
6) The pressure and density distributions are then calculated:

$$\begin{aligned} ln\left(\frac{P(r)}{P_{in}}\right) + B^*\left(P(r) - P_{in}\right) \\ + \frac{C^*}{2}\left(P(r)^2 - P_{in}^2\right) = \frac{\omega_e^2 r_{vt}^2}{2R_s T_{in}}\left(\frac{r^2}{r_{vt}^2} - 1\right) \end{aligned} \tag{9}$$

$$\rho(r) = \frac{P(r)}{R_s T_{in}\left(1 + B^* P(r) + C^* P(r)^2\right)} \tag{10}$$

7) The axial cold exit velocity (m/s) is computed.

$$u_z = \frac{\dot{m}_c}{\int_0^{2\pi}\int_0^{r_c} \rho(r) r \partial r \partial\theta} \tag{11}$$

where $\dot{m}_c$ is the cold mass flow rate (kg/s) and θ is the rotational angle.
8) The cold exit static enthalpy is calculated using P_c and T_c.
9) The cold exit total enthalpy (J/kg) is calculated using the following equation:

$$h_{0c} = h_c + \frac{u_z^2}{2} + \frac{u_z}{\dot{m}_c}\int_0^{2\pi}\int_0^{r_c} \frac{u_\theta^2(r)}{2}\rho(r) r \partial r \partial\theta \tag{12}$$

10) Then, the entropy of the cold exit is calculated.
11) Using the calculated value of h_{0c} from Eqn. (12) and the cold exit entropy, the total cold exit temperature (T_{0c}) is computed.
12) The hot exit total enthalpy is calculated using the conservation of energy:

$$h_{0h} = \frac{h_{0in} - \mu_c h_{0c}}{(1 - \mu_c)} \tag{13}$$

where $\mu_c = \frac{\dot{m}_c}{\dot{m}_{in}}$ and $\dot{m}_{in}$ is the inlet mass flow rate (kg/s).
13) To calculate the hot exit temperature (T_{0h}), CoolProp is used with h_{0h} and P_h being its inputs. When Zhu [19] measured the hot exit temperature, he regarded that the

total temperature is the same as the static temperature due to the low flow speed. Also, Camiré [20] neglected the hot exit speed and he attributed that to the fact that the forced vortex assumption becomes invalid near the hot exit due to wall friction. In addition to that, the hot exit area is much bigger than those of the inlet and cold exit and, hence, the velocity is much lower [20].

B. Losses and Corrections

The considerations of losses and corrections proved to be effective in closing the gap between the model predictions and the experimental data as shown by Lagrandeur et $al.$ [21]. Hence, some of these considerations that proved to have a significant effect are taken into account in the present work. The first improvement concerns the Bödewadt boundary layer flow which is important especially within the small cold mass fraction range. The approximated Eqn. (14) developed by Gutsol [22] is used as a simple representation of the mass flow rate escaping from the inlets to the cold exit.

$$\dot{m}_{bl} = 25 r_c \rho(r_c) \sqrt{\left[(r_{vt} - r_c)\, \nu \omega_e r_{vt}\right]} \tag{14}$$

where ν is the fluid kinematic viscosity (m^2/s).

In addition, the correction of the cold exit temperature made by Lagrandeur et $al.$'s [21] in order to avoid that T_{0h} may approach infinity at high cold mass fractions is considered. However, the correction is applied to h_{0c} instead of T_{0c} as seen in Eqn. (15) since the ideal gas assumption is not valid here. Then, using CoolProp, the temperature could be found.

$$h_{0c} = h_{0in} - (h_{0in} - h_{0u}) \tanh\left(A\,(1 - \mu_c)\right) \tag{15}$$

h_{0u} is the cold exit enthalpy computed by their original model while A is a scaling factor ($A = 2$) that controls the transition value between 0 and 1 of the tanh function.

III. Results

TABLE I
Operating parameters of the experimental studies of Camiré [20] and Zhu [19]

Parameter	Air	R134a	CO_2
P_{0in} (kPa)	239	903 - 1269	356 - 1883
T_{0in} (K)	294.6 - 295.6	323.5 - 324.8	293.8 - 297.3
$\dot{m}$ (g/s)	8.16 - 9.45	9.7 - 14.8	2.1 - 10
L (mm)	609.6	81.6	81.6
r_{vt} (mm)	12.7	6.3	6.3
r_c (mm)	4.15	2.9	2.9
No. of nozzles	4	6	6

In order to validate the real gas model developed here, several validations including three different refrigerants, namely air, R134a and carbon dioxide, are performed. The experimental data of Camiré [20] are used to compare results with air, while Zhu's [19] experimental data are used to compare results for both carbon dioxide and R134a. Also, the developed real gas model predictions are compared to those of Lagrandeur et $al.$ [21] using an ideal gas model. Table I presents the operating conditions and characteristics of the vortex tubes used in the different experiments. It must be noted that $r_{vc} = r_{vt}$ in all experiments.

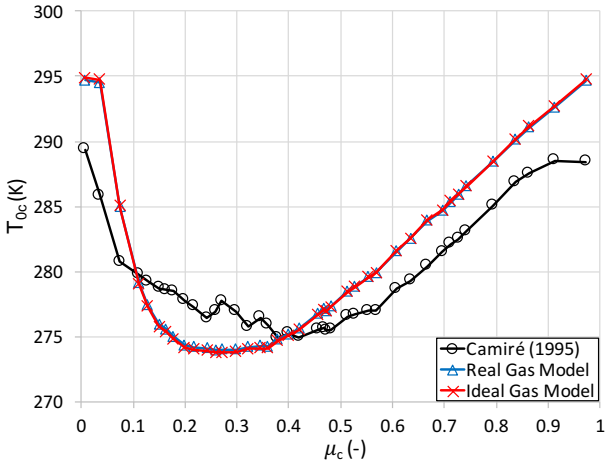

Fig. 2. Cold exit temperature prediction against Camiré's experiments [20] using air

Fig. 2 presents the predictions of the cold exit temperature against the experimental data of Camiré [20] for a vortex tube working with air. Both models provide almost identical results for the whole range of cold mass fraction. This is expected since air behaves as an ideal gas and barely deviates from this assumption within these operating conditions. The calculated compressibility factor is about 0.99. When comparing the results, the real gas model shows a maximum error of about 3% at cold mass fractions lower than 0.1. The model, then, underestimates the values between $\mu_c = 0.1$ and 0.5. Afterwards, it overpredicts the values but with a low error of up to 1.5% only till almost $\mu_c = 0.9$.

Fig. 3 displays the corresponding predictions for the hot exit temperature. Both models show a very decent agreement together but the real gas model starts to show better results after a cold mass fraction of about 0.7. This deviation can account for up to 1 K difference between both models. The reason is that the way the hot exit temperature is calculated by the real gas model is slightly different from that of the ideal gas model as it was previously evoked. The model underpredicts the T_{0h} values for cold mass fractions up to 0.25. It then starts to overpredict T_{0h} and the error between the experimental data and the model increases almost linearly. A maximum error of 3.5% is reached at a cold mass fraction of about 0.97. However, between cold mass fractions of 0.15 and 0.63, the model provides errors below 1.2%.

Fig. 4 shows the cold exit temperature calculations against Zhu's [19] experiments with R134a. Contrary to Camiré [20], the data of Zhu have not been obtained for a fixed parameter such as the inlet pressure. However, the presented results give a very good idea about both models' predictions. The real gas model exhibits a very good consistency in the prediction of

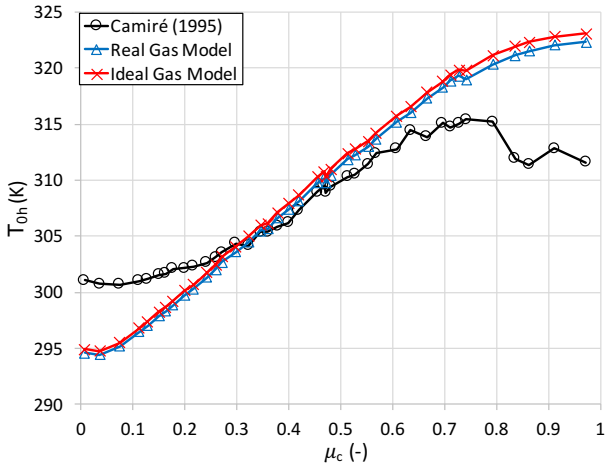

Fig. 3. Hot exit temperature prediction against Camiré's experiments [20] using air

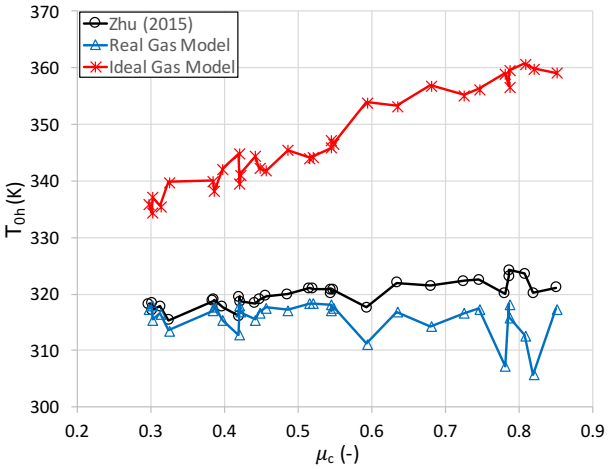

Fig. 5. Hot exit temperature prediction against Zhu's experiments [19] using R134a

the experimental results. However, even though the ideal gas model shows better predictions for cold mass fractions in the range $[0.55 - 0.75]$, it shows inconsistency in the predictions. The reason behind this is that the operating conditions of R134a are far from the ideal gas behavior. The calculated compressibility factor for the operating data points ranges from 0.85 to 0.89. The maximum error between the real gas model prediction and the data is around 1.67% only at a cold mass fraction of 0.781 and inlet pressure and temperature of 1261 kPa and 324.15 K, respectively. Using the ideal gas model, the highest error reached is about 4.1% at a cold mass fraction of 0.819 and inlet pressure and temperature of 1269 kPa and 323.95 K, respectively.

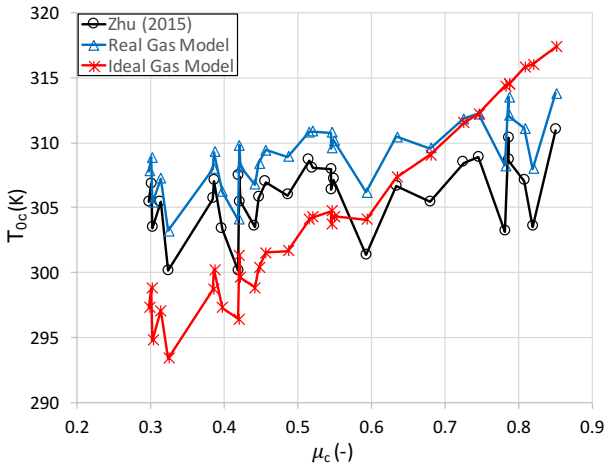

Fig. 4. Cold exit temperature prediction against Zhu's experiments [19] using R134a

Fig. 5 shows the hot exit temperature predictions of both models against Zhu's [19] R134a data. The results are different than those for the cold exit temperature. The ideal gas model overpredicts the temperatures by a large margin from the experimental data with a minimum error of around 5% at a cold mass fraction of 0.3 and inlet pressure and temperature of 923 kPa and 323.65 K, respectively. For the real gas model, the results are much better with a maximum error of about 4.5% only at a cold mass fraction of 0.819 and inlet pressure and temperature of 1269 kPa and 323.95 K, respectively. Two reasons can justify this significant difference between both models. The first, as mentioned above, is the non ideal behavior of R134a and the second is the differences in the calculation of the hot exit temperature.

As a last step of validation, Figs. 6 and 7 display the model predictions in terms of cold and hot exit temperatures, respectively, versus the carbon dioxide data of Zhu [19]. For most of the results, the real gas model shows better agreement with the experimental data than the ideal gas model. The maximum error between the real gas model and the experiments in the calculation of the cold exit temperature is about 4.3% at a cold mass fraction of 0.17 at inlet pressure and temperature of 387 kPa and 296.05 K, respectively. On the other hand and at the same conditions, the ideal gas model shows a maximum error of around 6.4%. Both models demonstrate that regardless of the inlet conditions, the agreement with the experimental data becomes better as the cold mass fraction increases.

Considering the hot exit temperature, the real gas model shows a very good agreement for all cold mass fractions lower than 0.63. However and regardless of that, the maximum error between the real gas model and the experiments is about 2.8% at a cold mass fraction of 0.67. The real gas model shows closer difference with the experimental data in comparison to the ideal gas model for every experimental data point. This behavior is similar to that of R134a and the explanations for that remain the same. However, the carbon dioxide's deviation from ideality is slighter than that of R134a [16]. The compressibility factor range for the presented data is $[0.9 - 0.98]$.

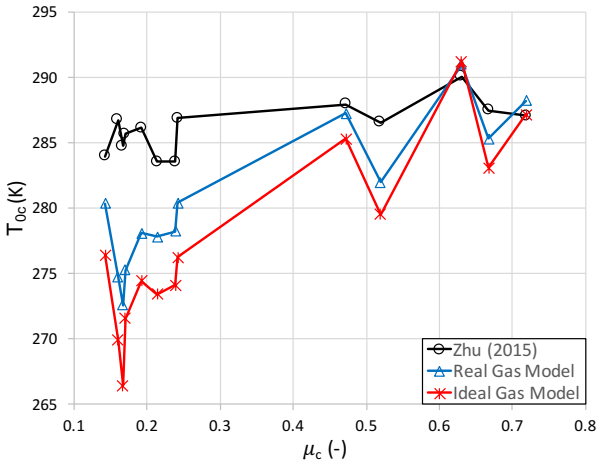

Fig. 6. Cold exit temperature prediction against Zhu's experiments [19] using carbon dioxide

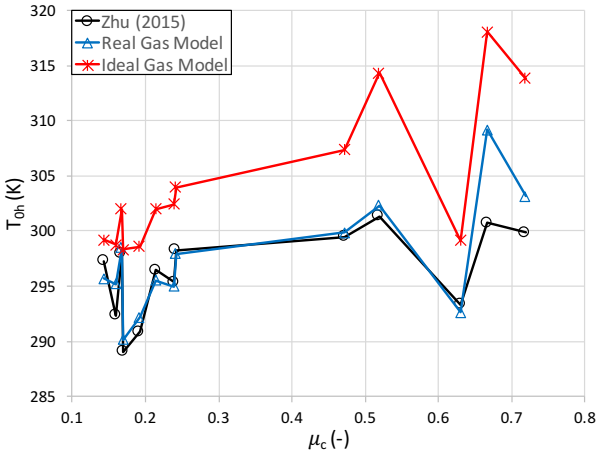

Fig. 7. Hot exit temperature prediction against Zhu's experiments [19] using carbon dioxide

IV. Conclusions

In this work, a new real gas model based on the virial equation of state was developed in order to calculate the exit temperatures of vortex tubes. Afterwards, the predictions were systematically compared to the ideal gas model recently proposed by Lagrandeur et al. [21]. The results were also compared to the experimental data of Camiré [20] for air vortex tubes and Zhu [19] for vortex tubes working with R134a and carbon dioxide. Both models exhibited similar performances for the exit temperatures of vortex tubes working with air. However, the real gas model significantly improved the predictions of the perfect gas model for the two other refrigerants. More comparisons are now suitable to further validate the model against experimental data for other refrigerants like hydrogen and also at very high pressures. As a future work, the present model will be used to optimize a transcritical CO_2 heat pump integrating a vortex tube.

Acknowledgments

The authors acknowledge the NSERC chair on industrial energy efficiency established in 2019 at Université de Sherbrooke with the support of Hydro-Québec, Natural Resources Canada and Emerson Commercial and Residential Solutions.

References

[1] G.J. Ranque. Experiments on expansion in a vortex with simultaneous exhaust of hot air and cold air. Journal de Physique et le Radium, 4(7): 112–114, 1933.

[2] R. Hilsch. The use of the expansion of gases in a centrifugal field as a cooling process. The Review of Scientific Instruments, 18(2): 108–113, 1947.

[3] U. Gupta, and M. Joshi. Experimental performance evaluation of counter flow vortex tube. Journal of Environmental Research And Development, 7(1), 2012.

[4] A.M. Crocker, S.M. White, and F. Bremer Jr. Experimental results of a vortex tube air separation for advanced space transportation, in: 39th Joint Propulsion Conference and Exhibit, Huntsville, USA, 20–23 July 2003.

[5] C.D. Fulton. Ranque's tube. Refrigerating Engineering, 5: 473–479, 1950.

[6] Y. Xue, M. Arjomandi, and R. Kelso. A critical review of temperature separation in a vortex tube. Experimental Thermal and Fluid Science, 34(8) :1367 – 1374, 2010.

[7] B. Ahlborn, and S. Groves. Secondary flow in a vortex tube, Fluid Dynamics Research, 21(2): 73–86, 1997.

[8] M. Kurosaka. Acoustic Streaming in Swirling Flow and the Ranque—Hilsch (Vortex-Tube) Effect. Journal of Fluid Mechanics, 124: 139–72, 1982.

[9] H.R. Thakare, and A.D. Parekh. Computational analysis of energy separation in counter—flow vortex tube, Energy, 85: 62-77, 2015.

[10] N. Agrawal, S.S. Naik, and Y.P. Gawale. Experimental investigation of vortex tube using natural substances, International Communications in Heat and Mass Transfer, 52: 51-55, 2014.

[11] S.E. Rafiee, and M.M. Sadeghiazad. Three-dimensional numerical investigation of the separation process in a vortex tube at different operating conditions. Journal of Marine Science and Application, 15: 157–165, 2016.

[12] V. Kirmaci, O. Uluer, and K. Dincer. An Experimental Investigation of Performance and Exergy Analysis of a Counterflow Vortex Tube Having Various Nozzle Numbers at Different Inlet Pressures of Air, Oxygen, Nitrogen, and Argon. Journal of Heat Transfer, 132(12): 121701, 2010.

[13] R. Liew. Droplet behaviour and thermal separation in Ranque-Hilsch vortex tubes. PhD thesis, Technische Universiteit Eindhoven, The Netherlands, 2013.

[14] R. Liew, J.C.H. Zeegers, J.G.M. Kuerten, and W.R. Michalek. Maxwell's demon in the Ranque-Hilsch vortex tube. Physical Review Letters, 109(5): 054503, 2012.

[15] A.V. Khait, A.S. Noskov, A.V. Lovtsov, and V.N. Alekhin. Semi-empirical turbulence model for numerical simulation of swirled compressible flows observed in Ranque–Hilsch vortex tube, International Journal of Refrigeration, 48: 132-141, 2014.

[16] Y.A. Çengel, and M.A. Boles. Thermodynamics: An Engineering Approach. McGraw-Hill Education, New York, USA, 8th Editon, 2015.

[17] J.H. Dymond, K.N. Marsh, R.C. Wilhoit, and K.C. Wong. Virial Coefficients of Pure Gases, Edited by M. Frenkel and K. N. Marsh, Springer, Berlin, Germany, Vols. 21A and 21B, 2003.

[18] J.L. Sengers, M. Klein, and J. Gallagher. Pressure-Volume-Temperature Relationships of Gases Virial Coefficients, National Bureau of Standards, Washington D.C., USA, 1971.

[19] J. Zhu. Experimental investigation of vortex tube and vortex nozzle for applications in air-conditioning, refrigeration, and heat pump systems. Master's thesis, University of Illinois at Urbana-Champaign, USA, 2015.

[20] J. Camiré. Experimental investigation of vortex tube concepts. Master's thesis, University of British Columbia at Vancouver, Canada, 1995.

[21] J. Lagrandeur, S. Poncet, M. Sorin, and M. Khennich. Thermodynamic modeling and artificial neural network of air counterflow vortex tubes. International Journal of Thermal Sciences, 146: 106097, 2019.

[22] A.F. Gutsol. The Ranque effect. Physics-Uspekhi, 40(6): 639–658, 1997.